A new global high resolution wave model for the tropical ocean using WAVEWATCH III version 7.14

Axelle GAFFET[1,2], Xavier BERTIN[2], Damien SOUS[3,4], Héloïse MICHAUD[5], Aron ROLAND[6], and Emmanuel CORDIER[7]

[1]Créocéan, Zone Technocean - Chef de Baie, 10 Rue Charles Tellier, 17000 La Rochelle, France.
[2]UMR 7266 LIENSs, CNRS-La Rochelle Université, 2 Rue Olympe de Gouges, 17000 La Rochelle, France.
[3]Université de Pau et des Pays de l'Adour, E2S-UPPA, SIAME, 64600 Anglet, France.
[4]MIO, Université de Toulon, Bâtiment F, 83130 La Garde, France.
[5]Shom, 42 Avenue Gaspard Coriolis, BP 45017 - 31032 Toulouse CEDEX 5, France.
[6]BGS IT & E, Darmstadt, Hesse, Germany.
[7]Observatoire des Sciences de l'Univers de La Reunion (OSU-Réunion), UAR 3365, Université de La Réunion, CNRS, IRD, Météo France, Saint-Denis, France.

Correspondence: Axelle GAFFET (axelle.gaffet@univ-lr.fr)

Abstract. Climate change is driving sea-level rise and potentially intensifying extreme events in the tropical belt, thereby increasing coastal hazards. In tropical islands, extreme sea levels and subsequent marine flooding can be triggered by cyclones but also distant-source swells. The knowledge of sea states in the tropical ocean is thus of key importance and their study is usually based on spectral wave models. However, existing global wave models typically employ regular grids with a coarse resolution, which fail to accurately represent volcanic archipelago, a problem usually circumvented by the use of obstruction grids but typically resulting in large negative biases. To overcome this problem, this study presents a new global wave model with a focus on distant-source swells, which received less attention than waves generated by cyclones. To accurately simulate sea-states in tropical areas, we have implemented the spectral wave model WAVEWATCH III© (WW3) over a global unstructured grid with a spatial resolution ranging from 50 km to 100 m. The model is forced by ERA5 wind fields, corrected for negative biases through a quantile-quantile approach based on satellite radiometer data. The wind input source terms adjusted accordingly and the explicit representation of tropical islands result in improved predictive skills in the tropical ocean. Moreover, this new simulation allows for the first time direct comparisons with the *in situ* data collected on volcanic islands at water depths ranging from 10 m to 30 m, which corresponds to a few hundred meters from shore.

1 Introduction

Over the last decades, coastal hazards have increased due to climate change, which causes sea-level rise as well as a possible intensification of extreme events in the tropical belt that can lead to more frequent marine floodings (Oppenheimer et al., 2019). Recent studies have even suggested that some low-lying islands and atolls could become uninhabitable by 2060-2090 due to annual flooding (Giardino et al., 2018). In addition, rising sea surface temperatures and ocean acidification exert strong pressure and locally degrade coral reefs, increasing the exposure of coastal islands to extreme events (Gattuso et al., 2014).

In tropical islands, extreme sea levels commonly result from storm surges, driven by the combination of atmospheric perturbations associated with tropical cyclones with a wave setup due to wave dissipation over reefs (Kennedy et al., 2012). Extreme sea levels can also develop apart from cyclones due to distant-source swells (hereafter DSS) (Hoeke et al., 2013). DSS are generated by remote storms developing several thousand kilometers away from the tropical belt, with the resulting DSS then propagating toward tropical coasts (Munk et al., 1997; Delpey et al., 2010; Smithers and Hoeke, 2014). DSS are less studied than cyclonic waves but their importance to coastal hazards was demonstrated at several tropical islands such as La Reunion Island (Lecacheux et al., 2012), French Polynesia (Canavesio, 2019; Andréfouët et al., 2023), Hawaii (Stopa et al., 2016), Marshall islands (Ford et al., 2018; Giardino et al., 2018) and British Virgin Islands (Cooper et al., 2013). It is worthwhile to highlight that, by contrast to cyclonic events associated to strong local winds and drop in atmospheric pressure, strong DSS events are able to impact and to damage the shore by physical processes solely driven by wave action (wave-setup, wave-driven currents, direct wave impact or long wave generation).

To accurately represent the propagation of DSS over thousands of kilometers, from the swell source in high latitudes to the tropical oceans, global spectral models are nowadays the most efficient approach. Spectral models describe the space and time evolution of the wave energy spectrum, using a phase-averaged approach that typical employ a resolution of tens of kilometers in the deep ocean. However, the accurate representation of wave field around and within archipelagos made up of islands only a few km-wide requires to reach a much finer resolution. To simulate the effect of small islands on the wave field while keeping computational times acceptable on a global scale, two approaches were developed. The first one uses an obstruction mask technique, which is only applicable to structured grids. In this approach, the percentage of land within each cell is used as a coefficient to calculate the attenuation of the wave action flux through the considered cell (Tolman, 2003). The second approach is based on a source term that considers both the attenuation of the wave action flux through the considered cell and its shadowing effect on the downstream cells. This method can be used for structured and unstructured grids (Mentaschi et al., 2018).

However, state-of-the-art hindcasts usually exhibit substantial negative biases around archipelago, suggesting that these techniques result in excessive wave energy loss (Rascle and Ardhuin, 2013; Dutheil et al., 2020). To overcome this issue, models using unstructured grids present an interesting potential since they allow small islands to be explicitly represented by locally refining the mesh. Unstructured grids have been first applied using explicit schemes, but the resulting high computational cost restricted this approach to regional areas (Roland, 2008; Roland and Ardhuin, 2014; Monteiro et al., 2022). Through the adoption of implicit schemes which enable to overcome the CFL constraint and significantly reduce simulation duration (Abdolali et al., 2020), unstructured grids slowly started to be used at a global scale (Brus et al., 2021; Mentaschi et al., 2023). Yet the spatial resolution used in these studies remains too coarse to allow for a direct validation around volcanic tropical islands because available *in situ* data, coming from wave buoys or bottom-moored pressure sensors, are usually located very close to shore (i.e. less than one km) due to the steep seabed slope around islands. Aiming to improve our capacity to accurately simulate sea states in tropical areas, we setup a new global spectral wave model based on an unstructured grid with a resolution ranging from 50 km to 100 m. Such fine resolution is set to allow for direct comparisons with measurements available by water depth of 10 to 30 m, that is very close to shore. The subsequent sections of this paper are structured as follows. First, we

describe the spectral wave model, its implementation and the observational data used for model validation at global and coastal scales. The section 3 highlights the model improvements through wind field corrections and the explicit representation of small islands both in the deep ocean and in the nearshore. Finally, we discuss the added value and limitations of the present approach, including the remaining challenges associated with spectral wave modeling on unstructured grids in tropical area.

2 Material and methods

2.1 Global wave models

2.1.1 Model description

Spectral wave models such as WAVEWATCH III© (WW3 Development Group, 2019) are typically used for large-scale applications, including operational or academic purposes. Spectral models are increasingly being applied to coastal areas, thanks to the development of unstructured grids versions, the better representation of coastal physics and the development of adaptive numerical schemes and integration strategy. In this work, we evaluate the performances of the model to simulate the sea states in the tropical ocean, using version 7.14 of WW3.

WW3 calculates the evolution of the wave spectrum by solving the Wave Action Equation (Komen et al., 1996). The source terms of this equation represent several key processes involved in wave transformation. In deep water, wave generation by wind (S_{in}) and wave dissipation by whitecapping (S_{ds}) are computed according to Ardhuin et al. (2010). Nonlinear wave interactions (S_{nl}) are modeled using the Discrete Interaction Approximation (DIA) of Hasselmann et al. (1985). The sea-ice interactions follow Liu and Mollo-Christensen (1988); Liu et al. (1991); Ardhuin et al. (2015) for wave damping by ice (S_{ice}), and the approach of Moon et al. (2007) for scattering and dissipation by sea ice (S_{is}). In shallow water, three other source terms become important: wave dissipation by bottom friction (S_{bot}), represented here using the SHOWEX parameterisation of Ardhuin et al. (2003), the breaking-induced wave dissipation (S_{db}) which follows the formulation of Battjes and Janssen (1978) and nonlinear triad interactions modeled using the LTA model of Eldeberky (1996).

For structured grids, the spatial propagation is solved using the explicit third-order Ultimate Quickest scheme (Leonard, 1991). This scheme is robust and stable but is limited by the CFL constraint, which discards the possibility to employ a spatial resolution fine-enough to capture nearshore wave transformations at global scale. Implicit schemes can be used to avoid prohibitive calculation costs at regional scale, while maintaining good scalability (e.g., Booij et al., 1999) on large core and mesh refinement. The WW3 implicit scheme, used in many studies and operational applications (e.g., Abdolali et al., 2020, 2021; Alves et al., 2022), computes a non-split solution of the wave action equation using a block Gauss-Seidel (Ferziger and Peric, 2002) solver for source terms and advection, avoiding splitting errors associated with the usual fractional step method. Recently, the integration methods and the numerical limiter were reformulated following Hersbach and Janssen (1999). Under-relaxation (e.g., Moukalled et al., 2016) for the strong and nonlinear terms describing near-resonant triplet interactions and shallow water induced wave breaking was added. Additional improvements on parallelization were implemented (Roland,

2008; Abdolali et al., 2020). Here we use the domain decomposition methods based on ParMetis (Karypis, 2011), which is interfaced using PDLIB (Parallel Decomposition Library).

2.1.2 Model implementations

Two grids are implemented to assess the relevance of a new unstructured grid compared to a classical structured grid.

The unstructured grid (hereafter UG) is created using SMS (Aquaveo, 2014). The mesh totals 296,199 nodes, with a resolution ranging from 50 km in the deep ocean to about 1 km around most islands (Fig. 2). Around the selected validation sites (see Sect. 2.2.2), the spatial resolution ranges from 1000 to 500 m. At la Réunion Island, where pressure transducer data are available only 400 m from the shoreline, the spatial resolution was further refined to 100 m. Such a fine resolution allows the water depth in the model to match that of the pressure transducer, which is essential to provide a consistent comparison. All islands smaller than 10 km^2 were arbitrarily removed to limit CPU time. The periodic continuity between -180°and 180°is guaranteed through the modification of the grid connectivity table.

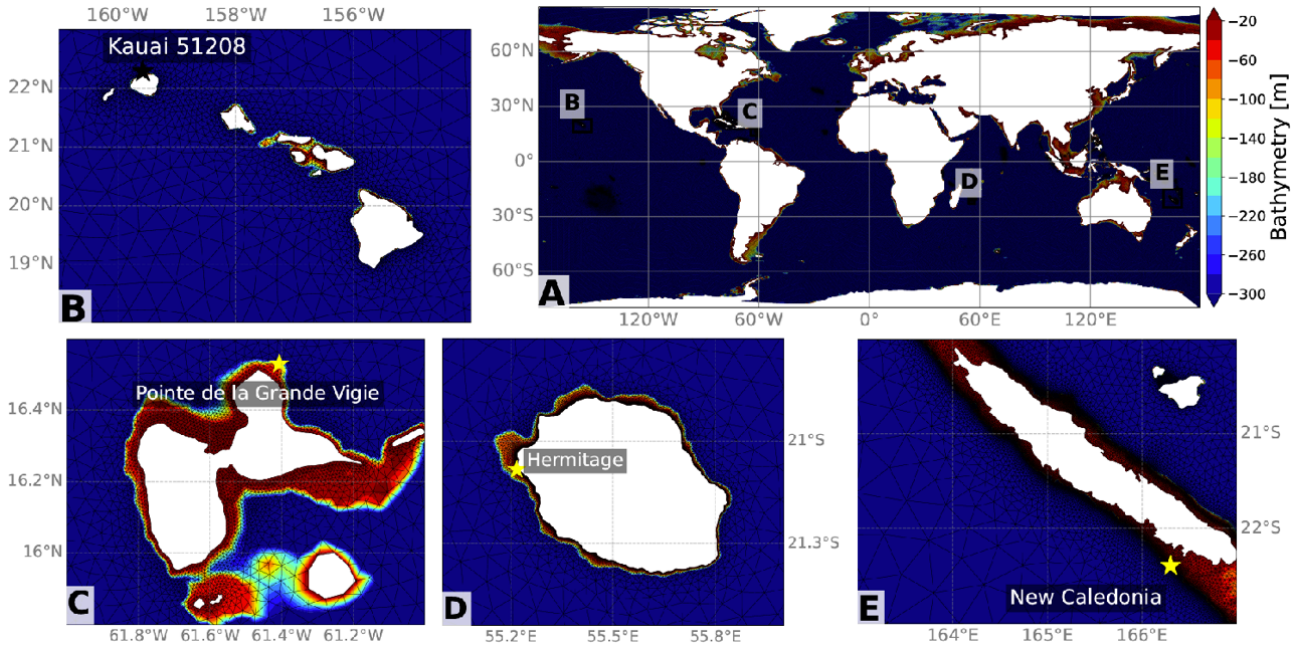

Figure 1. The global unstructured grid (A) with refinement at Hawaii (B), Guadeloupe (C), La Reunion (D) and New-Caledonia (E). The bathymetry is represented by the color legend.

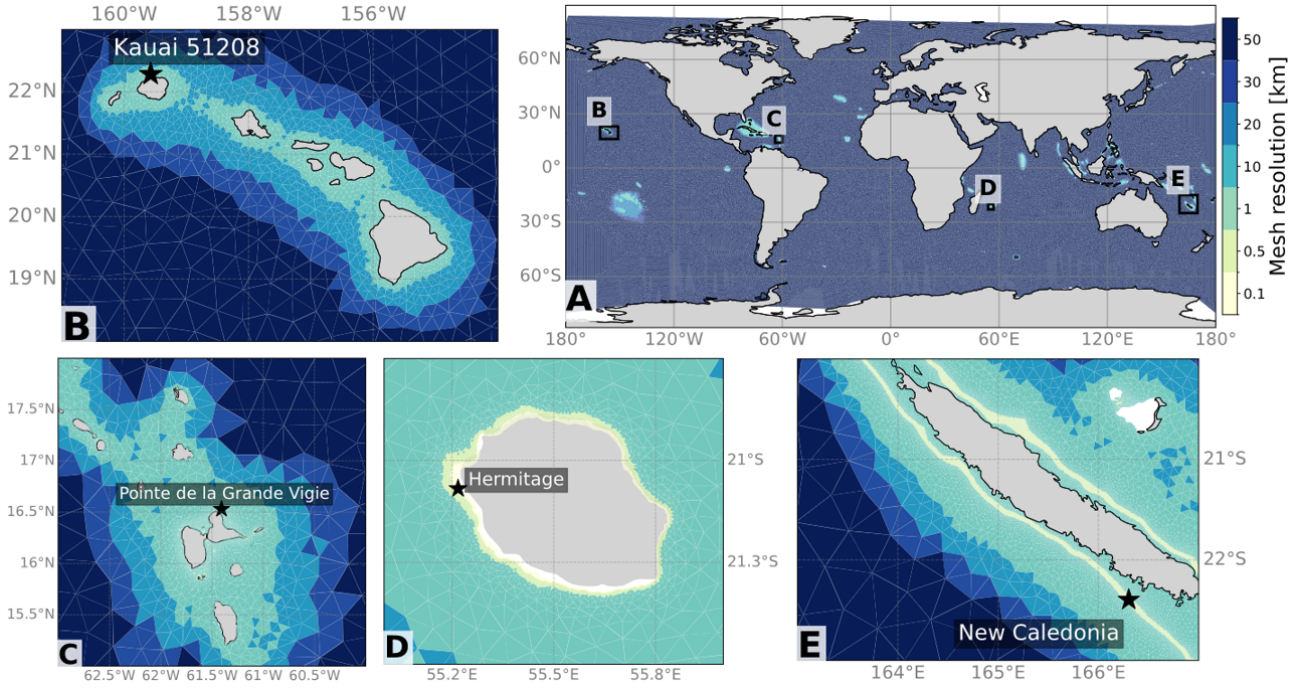

Figure 2. The global unstructured grid (A) with refinement at Hawaii (B), Guadeloupe (C), La Reunion (D) and New-Caledonia (E). The mesh resolution is represented by the color legend.

The structured grid (hereafter SG) has an uniform global resolution of 0.5°and islands smaller than the cell size are represented with an obstruction grid (Rascle and Ardhuin, 2013). The spectral grid consists of 24 directions and 36 frequencies logarithmically spanning the range 0.035-1.01 Hz (meaning a frequency interval exponent of 1.1). For SG, time steps are set to: 1350 s for global, 450 s for geographic advection and 600 s for spectral advection. The minimum time step for source term integration is 35 s. For UG, the implicit scheme does not require any splitting and a time step of 800 s is set. The global bathymetry comes from the General Bathymetric Chart of the Oceans (GEBCO) dataset (Weatherall et al., 2015). For UG, a higher resolution bathymetry is used around French tropical islands (New-Caledonia, La Reunion Island, Mayotte, French Polynesia, West Indies) originating from digital elevation models HOMONIM of 100 m resolution (Biscara and Maspataud, 2018).

Wind and ice forcing comes from the ERA5 reanalysis (Hersbach et al., 2020) with a 3-hourly time resolution and a spatial resolution of 0.5°globally. ERA5 also offers hourly data but sensitivity tests revealed similar results with 3 hourly wind fields. The ERA5 winds were preferred to the CFSR winds as they are more consistent over time (Liu et al., 2021). However, ERA5 winds are known to exhibit strong negative biases for the strongest winds (Pineau-Guillou et al., 2018; Campos et al., 2022). To solve this issue, Alday et al. (2021) proposed a correction of 5% of the wind speeds above 20 m/s and a new parameterisation of the source term in WW3 where the Betamax parameter, which controls the wave generation by the wind, is adjusted to 1.75. Our initial tests have shown that this approach reproduces well the most energetic sea states, but results in positive

biases for calmer conditions. Given that ERA5 winds are unbiased for light to moderate winds, we developed an alternative strategy, where wind fields are corrected using a quantile/quantile approach, based on wind fields estimates from radiometers as described by Bentamy and Croize-Fillon (2012) and available since 1992. The proposed correction is based on a piecewise multiplication factor displayed in Table 1:

Table 1. Wind speed and correction factor calculated through a quantile-quantile approach,based on wind fields estimates from radiometers

Wind speed [m/s]	**Correction factor [-]**
< 17	1
$17 < U_{10} < 20$	1.03
$20 < U_{10} < 23$	1.08
$23 < U_{10} < 26$	1.14
$26 < U_{10} < 30$	1.20
$U_{10} > 30$	1.27

As ERA5 wind fields were compared against radiometer data over different oceanic basins (Pacific, Indian, Atlantic) for selected 1-month periods (July 1996, May 2007, January 2014, respectively), encompassing major past swell events and enhanced very strong winds. In the Southern Pacific Ocean, a major storm in July 1996 produced one of the largest distant swells ever reported (Canavesio, 2019), with wind fields reaching 30 m/s (Fig. 3-C). In the Southern Indian Ocean, a strong storm in May 2007 produced winds over 30 m/s (Fig. 3-B), which drove a major distant swell (Lecacheux et al., 2012). Finally, in the NE Atlantic Ocean, winter 2014 exhibited an unprecedented succession of violent storms (Masselink et al., 2016), with several events driving winds over 35 m/s (Fig. 3-A). For these three periods and regions, the comparison confirms that ERA5 winds are unbiased for speed up to 15 m/s while for higher winds, the bias correction reaches 10% at 20 m/s and 15% at 25 m/s. Remarkably, this correction holds for all oceanic basins and time periods where the comparison is performed. Finally, the "Test471" parameterisation of Rascle and Ardhuin (2013) is used for the wind growth and whitecapping dissipation source terms, where the Betamax parameter has been adjusted to 1.43. The new parameterisation proposed in this study is hereafter called "`ERA5_QC`".

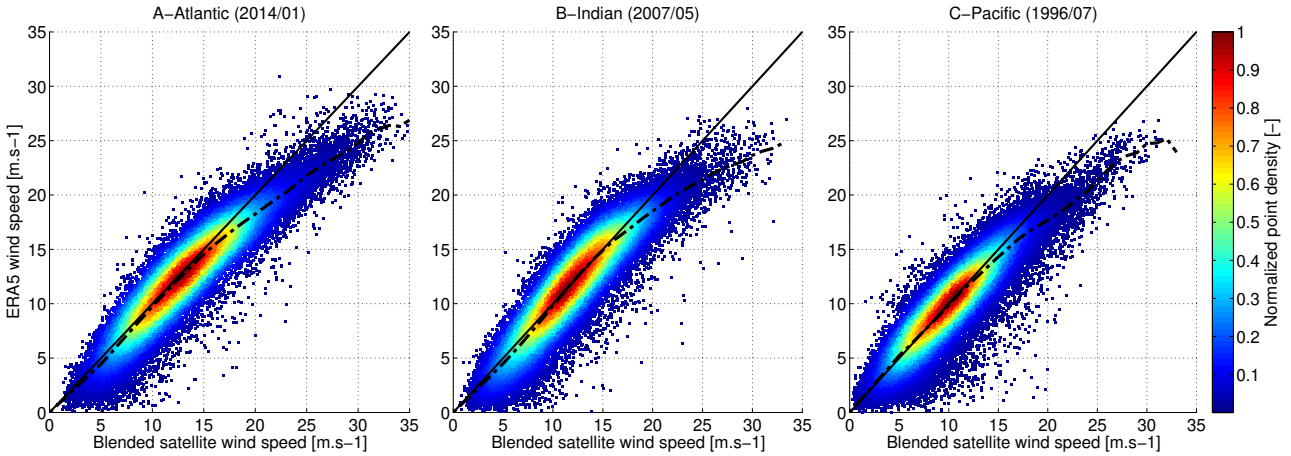

Figure 3. Comparisons between blended winds and ERA5 winds for A) The Atlantic ocean B) The Indian Ocean and C) The Pacific Ocean.

Other source terms are set to default settings.

2.2 Observational data

Altimetry data and *in situ* measurements are used for global and coastal validation, respectively.

2.2.1 Altimetry data for global validation

The model evaluation in the deep ocean is performed against the European Space Agency Climate Change Initiative (ESACCI) altimetry data (Dodet et al., 2020; Schlembach et al., 2021). The ESACCI dataset v3 used here was retrieved from multiple satellite missions spanning from 2002 to 2022. For the present model validation, an entire year (2007) is used to cover a wide range of sea states. The simulated significant wave height H_{m0} over the full spectral range is interpolated in time and space to match the satellite "denoised" significant wave height at approximately 6 km spatial resolution (Quilfen and Chapron, 2021; Schlembach et al., 2021). Both satellite data and interpolated WW3 outputs are averaged over 0.5°grid cells, which enables to calculate stable statistical values for the collocated satellite/model data. All satellite values out of the model time and space ranges were skipped. Coastal values in a 50 km range from the shoreline were flagged out due to possible coastline interference with the signal and the lack of model resolution along the coast.

2.2.2 Coastal and nearshore data

For each coastal/nearshore site, the model validation is performed over a four-month period, selected to represent a wide variability of wave conditions. The WW3 wave bulk parameters (H_{m0} and T_{m02}) are calculated from the modeled spectrum using a specific frequency cut-off, depending on the water depth or the device employed (see Table 2). For bottom pressure data, the nonlinear moderately dispersive reconstruction described by Martins et al. (2021) is employed. Wave bulk parameters are then computed using classical spectral analysis.

Table 2. Description of coastal and nearshore data used for model validation at the four study sites.

Name	Lat	Lon	Depth (m)	Data Type	High-Frequency Cutoff (Hz)	Validation Period	Mesh Resolution (km)
Hawaii/51208	22.285 N	159.574 W	200	Wave Buoy (Datawell WR)	0.62	Aug-Dec 2022	1
Guadeloupe/97103	16.536 N	61.407 W	90	Wave Buoy (Datawell WR)	0.62	Feb-Jun 2008	1
La Reunion	21.083 S	55.217 E	12	Pressure Sensor (RBR Duo)	0.25	Apr-Aug 2022	0.1
New-Caledonia/1402	22.397 S	166.303 E	11	Pressure Sensor (Seabird SB26Plus)	0.25	Mar-Jul 2020	0.5

For Hawaii (Pacific Ocean), the validation data are provided by the 51208 wave buoy from the National Data Buoy Center (NDBC) and the period from August to December 2022 was chosen due to the occurrence of high energetic events. The data are owned and maintained by the Pacific Islands Ocean Observing System (PacIOOS) and provided by the Scripps Institution of Oceanography. The buoy is located above Hanalei Bay, to the North of Kauai by 200 m water depth (see Fig. 1-B). For this buoy, only H_{m0} and T_p time series were available.

For Guadeloupe (Atlantic Ocean), the validation data are collected by the 97103 Candhis wave buoy from CEREMA (*Centre d'études et d'expertise sur les risques, l'environnement, la mobilité et l'aménagement*) and Météo-France. The period from March to July 2008 was chosen for validation due to the occurence of an extreme swell event (Lefèvre, 2009). The buoy is located in the French West Indies, above the Pointe de la Grande Vigie, Northeast of Guadeloupe by 90 m water depth (see Fig. 1-C).

For La Reunion Island (Indian Ocean), the pressure sensor data are collected continuously in the framework of the SNO *Service National d'Observation* ReefTEMPS (Cordier et al., 2024), operated by the OSU-Reunion. The period from April to August 2022, during which a strong swell event occurred, was chosen for validation. The pressure sensor is located in the reef slope in front of the Hermitage Beach, bottom-moored by a mean water depth of 12 m (see Fig. 1-D).

For New-Caledonia (Pacific Ocean), pressure sensor data were collected from October 2019 to November 2020 during the GEOCEAN-NC 2019 field campaign (Chupin et al., 2023). The pressure sensor was moored in the reef slope to the Southwest of the main island by a mean water depth of 11 m (see Fig. 1-E). The period from March to July 2020 was chosen for validation as it encompasses several energetic events.

Lastly, as the 3-hour resolution of the wind forcing does not allow to capture the high frequency wave variability, observational data were low-pass filtered with a 3 h window.

2.3 Validation metrics

Several metrics are used to assess the errors between modeled results and observational data, including the normalized mean square error (NRMSE) defined as:

$$\mathrm{NRMSE}(X) = \sqrt{\frac{\sum (X_{\mathrm{mod}} - X_{\mathrm{obs}})^2}{\sum X_{\mathrm{obs}}^2}} \tag{1}$$

where X_{mod} is the modeled result and X_{obs} the observed value and the normalized bias defined as:

$$\mathrm{NBIAS}(X) = \frac{\sum (X_{\mathrm{mod}} - X_{\mathrm{obs}})}{\sum X_{\mathrm{obs}}} \tag{2}$$

3 Results

3.1 Global validation in deep water

The model validation in deep water is first performed only on structured grids to evaluate the effect of wind field correction. Next, the evaluation of the spatial discretisation is carried out comparing SG and UG approaches, both including the wind correction.

3.1.1 Impact of wind field correction

Initial results with the parameterisation T475 of Alday et al. (2021) on SG show a global mean NRMSE of 14.1% and a global positive bias of 3.36% (see Fig. 4-A). Around island archipelagos (e.g French Polynesia, Indonesia, West Indies, Maldives), higher errors occur locally exceeding 30%. These larger errors are mostly associated to strong negative biases and are presumably linked to the obstruction grid. The implementation of the wind correction leads to better results, especially in the Atlantic, Indian and Pacific oceans, away from island areas, with a global NRMSE of 12.9% (Fig. 4-B). Strong positive biases are locally lowered which results in a global mean normalized bias of -4.4%.

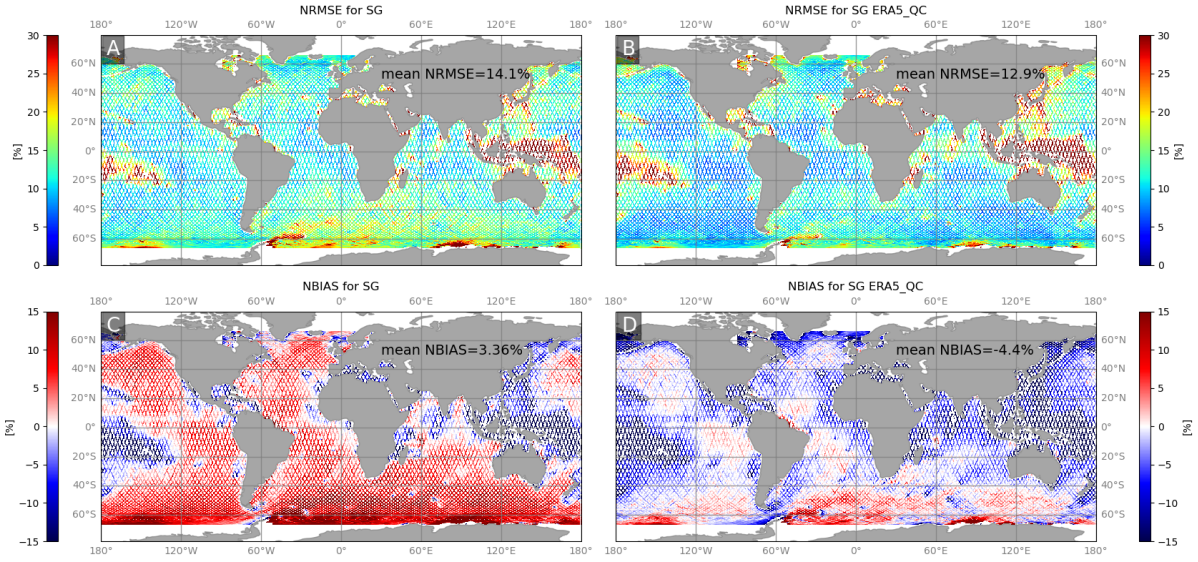

Figure 4. Normalized RMS error (A) and normalized bias (C) between H_{m0} deduced from altimetry and simulated with T475 parameterisation and normalized RMS error (B) and normalized bias (D) with `ERA5_QC` parameterisation.

3.1.2 Impact of spatial discretisation: SG versus UG

Figure 5 displays the comparison between SG and UG configurations, both employing `ERA5_QC`. The unstructured grid leads to a lower global NRMSE of 11.6% (see Fig. 5-B). Much stronger local improvements are observed around archipelagos all

around the globe. In SG, tropical archipelagos are generally associated with large NMRSE and strong negative bias. In UG, NRMSE is drastically reduced while the bias shifts to weakly positive. Restricting the NRMSE computation to the tropical band, between 23.27°N and 23.27°S, the error drops from 15.3% to 11% with the UG. The global mean normalized bias is considerably reduced to 1.5% with ERA5_QC parameterisation.

The results obtained globally for the UG ERA5_QC configuration will be further analyzed and discussed in Sect.4, where we investigate the implications of the remaining biases and their potential sources, particularly focusing on regions such as Antarctica, semi-enclosed seas, coastlines, the Mozambican channel, and the inner seas of Indonesia where higher errors persist.

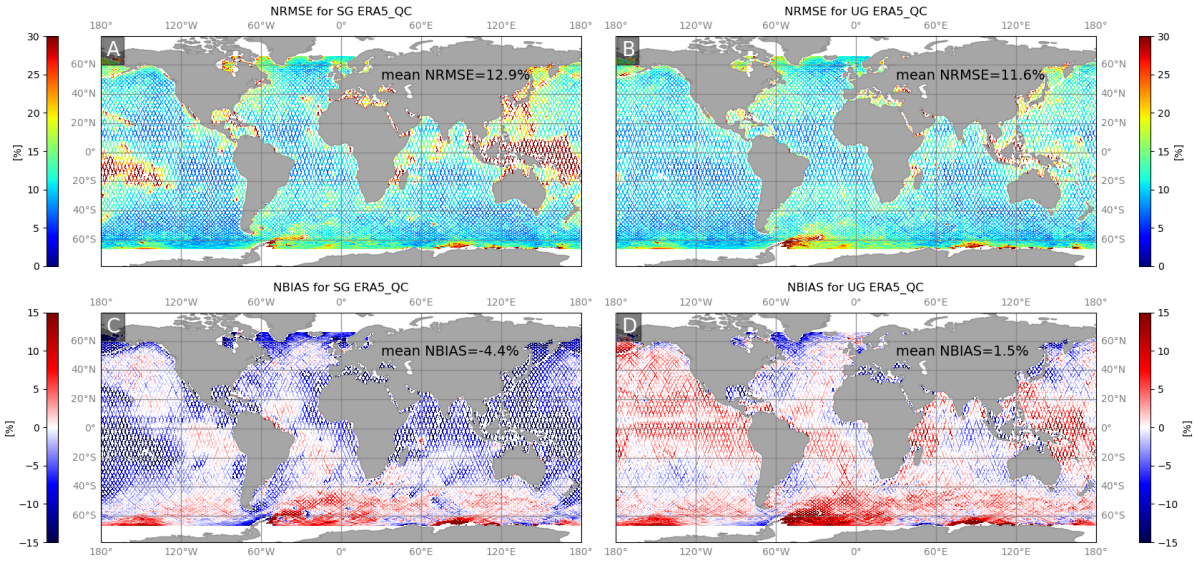

Figure 5. Normalized RMS error (A) and bias (C) between H_{m0} deduced from altimetry and simulated with the UG ERA5_QC configuration and normalized RMS error (B) and normalized bias (D) with the SG ERA5_QC parameterisation.

The distribution of the bias as a function of H_{m0} is shown on Fig. 6 for the three model configurations. With SG, the ERA5_QC parameterisation results in a lower bias compared to T475. Indeed, the T475 parameterisation uses a higher Betamax parameter, which controls the wind input term and hence the wave growth, set to 1.75 compared to 1.43 in the ERA5_QC parameterisation. This higher Betamax leads to greater wave growth and therefore a positive bias, although winds are lighter in the T475 than in the ERA5_QC. For the UG ERA5_QC, the bias is positive for H_{m0} between 1 and 2.5 m and the bias slowly decreases after and is negative for H_{m0} values ranging from 2.5 m to 12 m. The bias reaches its lowest value at -0.4 m for H_{m0} of 11 m. The observed lower biases for the SG and the ERA5_QC models in the 10-12 m wave bins will be discussed further in the paper.

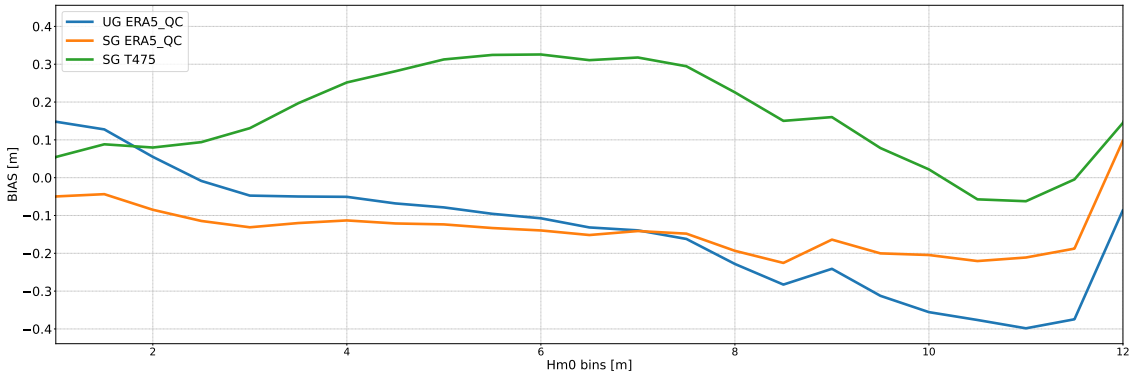

Figure 6. Distribution of the bias as a function of H_{m0} for each simulation (SG T475, SG `ERA5_QC` and UG `ERA5_QC`) for the year 2007 at global scale.

3.2 Example of coastal validation

Long-term *in situ* wave data are scarce in the nearshore area of tropical island bordered by steep slopes. The coastal validation of the model is carried out at four tropical islands: La Reunion in the Indian Ocean, Guadeloupe in the Atlantic Ocean, New-Caledonia and Kauai (Hawaii archipelago) in the Pacific Ocean. These islands are representative of steep-slope tropical islands exposed to multi modal sea states. For each island, *in situ* measurements are available by water depth ranging from 11 m to 200 m for periods over one year, allowing for the first time to evaluate the performance of a global wave model very close to shore.

3.2.1 La Reunion

Figure 7 displays the comparison between model and bulk parameters computed from pressure sensor data at La Reunion (12 m water depth) for H_{m0}, T_{m02} and T_p. Overall, the model is able to capture the variability of the sea state over the selected time period, including the extreme DSS of June 29th, 2022 where H_{m0} reached 7 m with T_p exceeding 21 s. The NRMSE for H_{m0} of 19.82% is similar to the NRMSE obtained in the deep ocean around La Reunion (see Fig. 5). The consistency between the results obtained globally and the results obtained in shallow water at the Hermitage demonstrates the ability of the model to represent the wave transformation from deep ocean to shallow area. H_{m0} tends to be slightly overestimated, which also matches the deep water bias in this region (Fig. 5). Wave periods are well represented with NRMSE of 9.31% and 8.29% for T_{m02} and T_p, respectively.

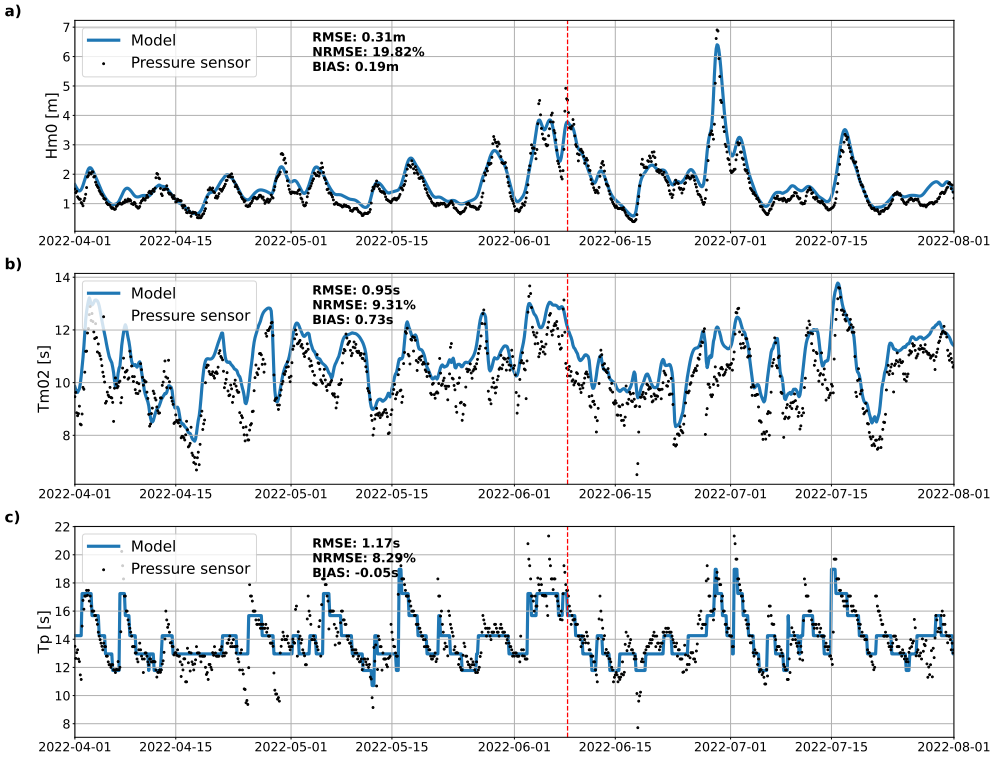

Figure 7. Wave bulk parameters derived from the pressure sensor against the model for April to August 2022 at Hermitage (La Reunion) for a) H_{m0} b) T_{m02} and c) T_p. The red line corresponds to a particular time where the PSD will be compared in the discussion.

3.2.2 Hawaii

Figure 8 shows the comparison between model and wave buoy data at Hawaii (200 m water depth) for H_{m0} and T_p. The general temporal evolution of the wave bulk parameters is correctly represented, with H_{m0} and T_p NRMSE of 15.82% and 12.99%, respectively. However, the peaks in H_{m0} tend to be underestimated by up to 1 m (see December, 20 event on Fig. 8). The discrepancies between modeled and observed T_p are generally related to quick shifts under multi-modal sea states, i.e. from DSS (T_p ranging from 10 s to 17 s) to local wind sea (T_p ranging from 5 s to 8 s) or conversely.

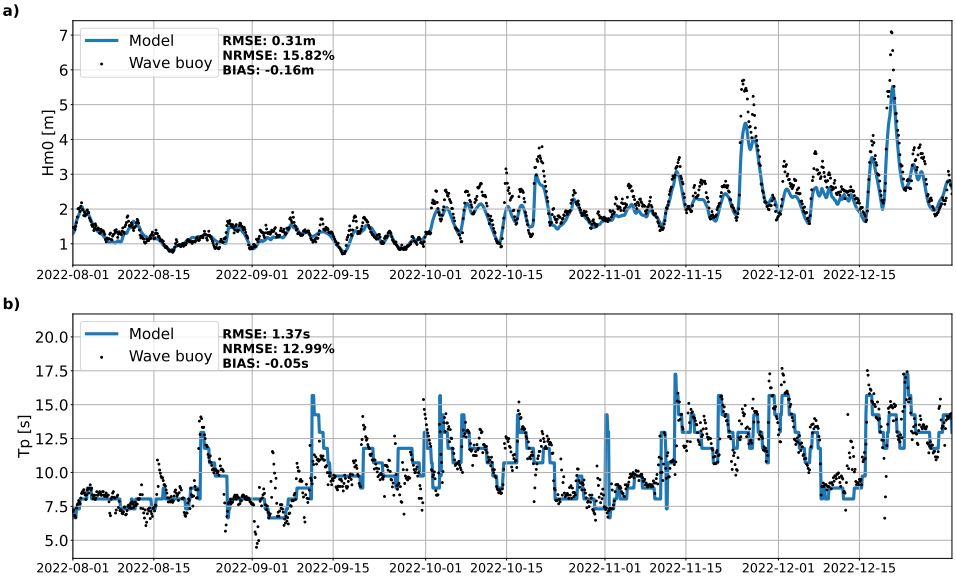

Figure 8. Wave bulk parameters estimated from wave buoy against model for August to December 2022 at Kauai (Hawaii) for: a) H_{m0} and b) T_p.

3.2.3 Guadeloupe

Figure 9 depicts the comparison between model and wave buoy data at Pointe de la Grande Vigie to the North of Guadeloupe (90 m water depth) in the Caribbean Sea for H_{m0}, T_{m02} and T_p. This figure reveals a very good behavior of the model with NRMSE under 12% for the wave bulk parameters. The strongest DSS event over the observed period (March to July, 2008) is correctly captured in terms of wave periods but the maximal H_{m0} peak is again underestimated by up to 1 m. This problem will be further discussed in this paper.

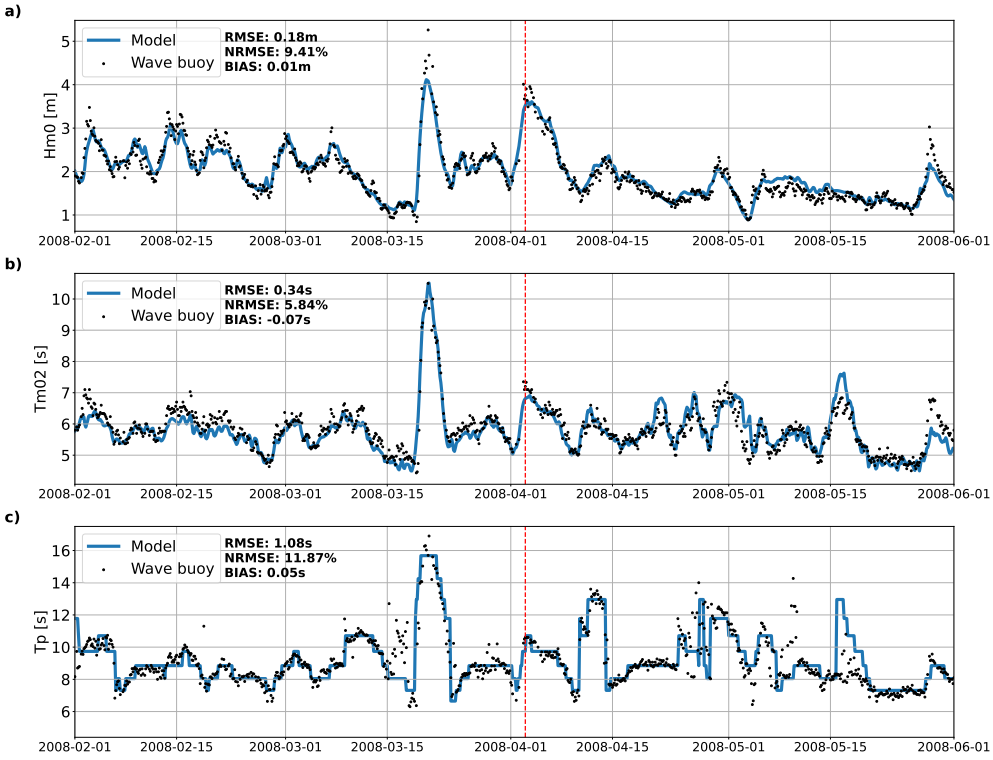

Figure 9. Wave bulk parameters derived from wave buoy against model for March to July 2008 at La Pointe de la Grande Vigie (Guadeloupe) for a) H_{m0} b) T_{m02} and c) T_p. The red line corresponds to a particular time where the PSD will be compared in the discussion.

3.2.4 New-Caledonia

Figure 10 displays the comparison between the model and the wave bulk computed from the pressure sensor data at Noumea (11 m water depth) for H_{m0}, T_{m02} and T_p. The NRMSE and bias for H_{m0} are 16.75% and 0.07 m, respectively. The periods are also correctly represented with NRMSE values of 7.92% and 14.09% for T_{m02} and T_p, respectively. Similarly to Kauai, rapid fluctuations in multi-modal sea states are difficult to represent in the model and result in higher error on T_p. More specifically, the peak of H_{m0} exceeding 4.5 m on 15 March 2020 is associated with the category 1 to 2 cyclone Gretel, which passed about 150 km to the southwest of New Caledonia. This event is accurately reproduced by the model, which suggests that the sea states associated with tropical cyclones can also be accurately simulated by our model.

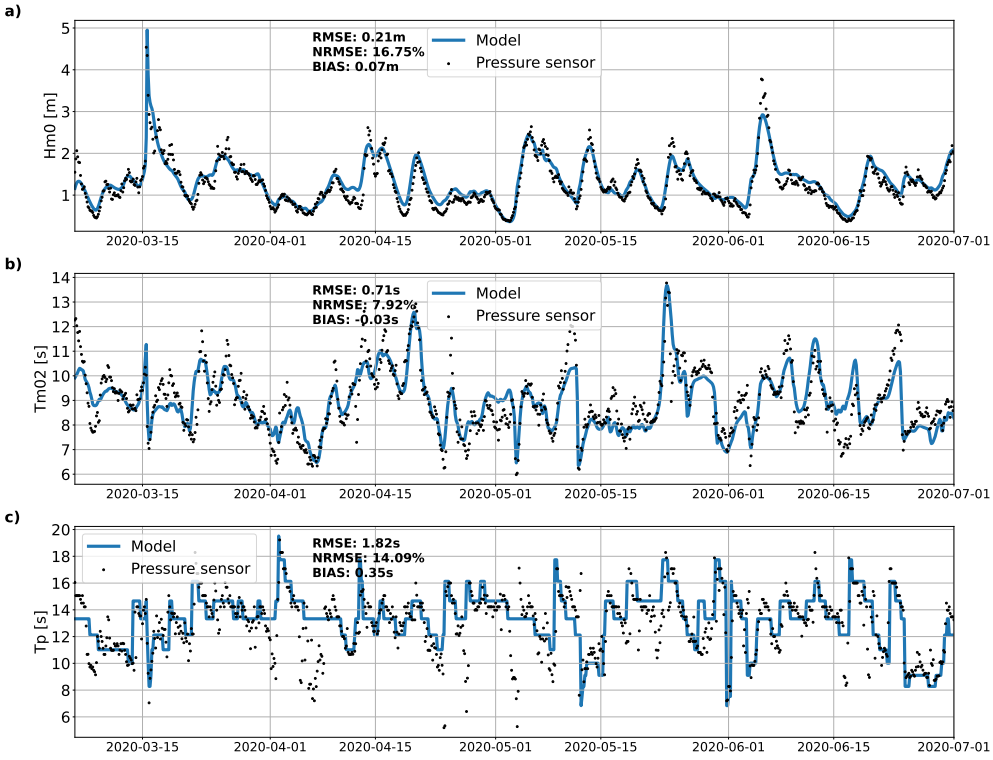

Figure 10. Wave bulk parameters estimated from pressure sensor against model for 2020 at Noumea (New-Caledonia) for: a) H_{m0} b) T_{m02} and c) T_p.

4 Discussion

4.1 Predictive skills and comparisons to existing global hindcasts

Focusing first on the sole wind correction by the quantile-quantile approach, better H_{m0} predictions are obtained compared to the results obtained with the wind correction and source term of Alday et al. (2021). The approach presented in this study reduces the positive bias present for calmer conditions and consequently improves the general wave representation. In more details, as seen in Fig 6, the uncorrected SG has a lower absolute bias than either of the `ERA5_QC` for the 10-12 m wave bins. Such large waves are driven by extreme winds (i.e. larger than 25-30 m/s), for which we have a limited number of observations, as can be seen on Fig. 3. Therefore, the quantile-quantile wind correction could be further improved for very high winds, provided more observations are available.

It should be mentioned that the comparison was performed using the same wind correction and source term as T475 but the whole configuration of the model presented in Alday et al. (2021) also included a multigrid approach, improved ice forcing and ocean current forcing. In our configuration, one single structured grid is used with standard ice forcing and no current effect. One can expect better results combining the comprehensive configuration of Alday et al. (2021) with our wind correction.

Existing hindcasts such as ERA5 can result in poor predictive skills when compared with coastal measurements (Samou et al., 2023). Similarly, coastal comparisons of the existing hindcasts ERA5-I and CFRS-W are limited by their global resolution of 0.3°and 0.5°, respectively (Stopa and Cheung, 2014). Global unstructured grid models emerged recently (Brus et al., 2021; Mentaschi et al., 2023), which avoid the use of the obstruction masks required for regular grids. However, the resolution employed in these studies also remains too coarse to allow for a direct validation in nearshore shallow depth. A few studies already compared global wave model with stations located by 10-30 m water depth, although these wave buoys were moored at gently sloping inner shelves or in big lakes (Zheng et al., 2016; Alday et al., 2021). The novelty here is that, due to the steep slopes usually surrounding volcanic islands where our stations are located, such water depths are found very close to shore, typically a few hundred meters. Specifically designed to simulate sea state around tropical islands, our new model is able to explicitly represent small islands and to reach a local resolution allowing a direct comparison with nearshore observations and a correct representation of wave transformation from deep to shallow water. Even multigrid system such as the ones described by Rascle and Ardhuin (2013) refined at 3' resolution or more recently Dutheil et al. (2020) and Alday et al. (2021), both refined at 0.05°are too coarse to make a direct comparison with coastal observations, often located only a few hundred meters from the coast.

4.2 Remaining challenges in deep water

However, despite these advances, areas such as polar regions, semi-enclosed seas, the Mozambique channel and the inner seas of Indonesia displays larger errors compared to the other ocean basins (Fig. 5). In polar regions such as the Antarctic, overestimated H_{m0} are likely related to inaccuracies in the representation of sea-ice dissipation, despite efforts to include icebergs (improvement of the NRMSE of 0.1% when the icebergs were added in the present model). The sea ice concentration in ERA5 remains uncertain, especially in the Marginal Ice Zone (MIZ) (Renfrew et al., 2021). The oversimplified parameterisation of wave propagation within sea ice areas does not take into account the calving and drifting of icebergs into the Southern Ocean, which causes significant blocking of the wave energy (Ardhuin et al., 2011; Khan et al., 2021). Moreover, the altimetry data used for model assessment can suffer inaccuracies in the presence of ice (Dodet et al., 2020).

Around coastlines and in semi-enclosed seas, model errors can result from wind inaccuracies associated with the land-sea transition (Xie et al., 2001; Chelton et al., 2004). In addition, the ERA5 wind is known to be less accurate in mountainous areas such as in the Mediterranean Sea, where the steep orography is misrepresented by the limited resolution of the reanalysis (Graf et al., 2019; Dörenkämper et al., 2020; Gutiérrez et al., 2024). Moreover, the spatial resolution and the representation of the strongest winds may limit our ability to accurately model hurricanes (Jullien et al., 2024), although model data comparison during cyclone Gretel off Nouméa (Fig 10) suggests that the associated sea states can be accurately simulated a few hundred kilometers away from the cyclone eye. In the Mozambique Channel, the higher errors are probably due to the fact that currents

are not represented in our model. Indeed, the strong Agulhas Current has a direct influence on the wave field propagation (Ardhuin et al., 2017). Similarly, in the Southern Ocean, accounting for the circumpolar current is known to significantly reduce the positive bias of the modeled wave height (Rapizo et al., 2018). Although currents are known to improve the model results (Marechal and Ardhuin, 2021), one of the main priorities was to produce a hindcast consistent over time. Considering that CMEMS-Globcurrent surface currents are only available from 1993, it was decided to neglect currents in the model.

Although the explicit representation of islands whose areas are larger than 10 km^2 in our UG considerably improves wave predictions in archipelago compared to obstruction grids, this threshold remains arbitrary. One can wonder if representing smaller islands could further improve the predictions, namely in areas with tens of thousands of islands such as Indonesia. A possible alternative would be to combine the present approach with obstruction grids for the smallest islands, following, for instance, the method of Mentaschi et al. (2018).

Keeping in mind these limitations, the present approach based on implicit schemes remains an efficient compromise to simulate the generation and propagation of sea states down to nearshore regions, while maintaining low computational cost. Modeling the sea states at global scale with fine refinement at coastal scales is hardly practical with explicit schemes as simulating one year with 200 cores takes over 50 h. The simulation presented in this study was only possible thanks to the use of implicit schemes which overcomes the CFL constraint, and therefore considerably reduces the simulation time (Abdolali et al., 2020). Indeed, for the same computational resources, a one year simulation with implicit scheme took 12 h. At the wave event scale, the H_{m0} peaks tend to be underestimated at some locations for the most energetic events. In order to investigate if this problem is already present in the deep ocean, Fig. 11 provides a comparison during the major 2007 DSS event between UG implicit and SG explicit results and data deduced from satellite altimetry. This comparison reveals a diffusion behaviour of the UG run with an underestimation of the peak up to 0.7 m. Indeed, a possible explanation for the underestimation of the peaks of H_{m0} can be the diffusion of the implicit schemes used for the UG (Roland and Ardhuin, 2014; Abdolali et al., 2020).

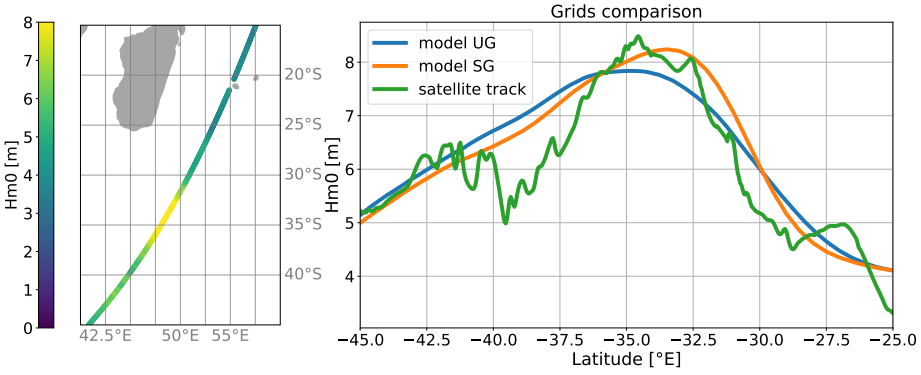

Figure 11. Comparisons between altimetry and modeled H_{m0} WW3 numerical schemes comparison at 52E, 25S during the major DSS on May 13th, 2007.

So far, the latest version of WW3 with implicit schemes was only tested and validated for hurricanes (Abdolali et al., 2020, 2022) with short fetches and relatively small propagation area compared to the DSS example considered here. Further research efforts are therefore required to develop new higher order implicit schemes able to reduce diffusion and better capture H_{m0} peaks. A second-order implicit scheme must remain positive and monotone, even at high CFL numbers, which is inevitable when increasing the resolution along the coasts. For example, the Crank-Nicholson time discretization maintains monotonicity only up to a CFL number of 2. Beyond this, achieving positivity and monotonicity becomes challenging because, according to the Godunov theorem, the scheme must be nonlinear.

In order to further investigate the discrepancies observed, a comparison between modeled and observed power spectral density is shown at Pointe de la Grande Vigie (see Fig. 12).

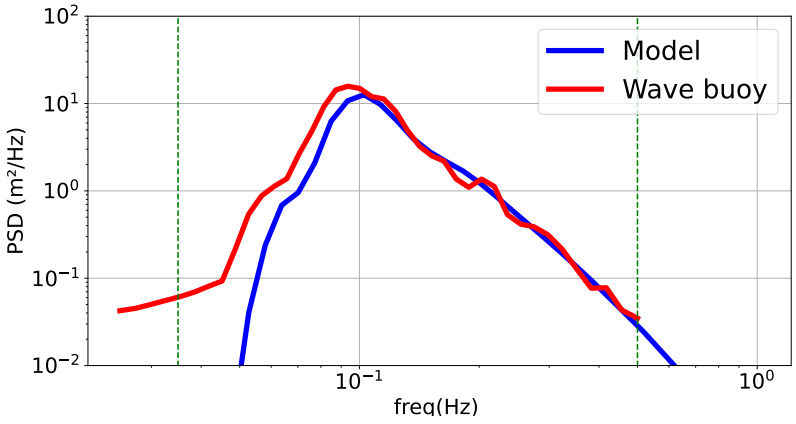

Figure 12. Comparison between power spectral density modeled and observed at 18:00 UTC on April 2nd, 2008 (Pointe de la Grande Vigie, Guadeloupe).

This comparison shows an underestimation of the wave energy spectrum between 0.04 Hz and the peak frequency. This underestimation can be due to the parameterisation of the nonlinear quadruplet wave interactions, which uses the Discrete Interaction Approximation (DIA) of Hasselmann et al. (1985). Although widely used, the DIA is a crude approximation as shown by Benoit (2007), Vledder et al. (2012) and Alday and Ardhuin (2023). Other alternative methods exist (Webb, 1978; Tracy and Resio, 1982; Hasselmann and Hasselmann, 1985; Masuda, 1980) but require very high computational costs and are therefore not practical with a global model. The underestimation of the wave energy spectrum below 0.04 Hz will be discussed in the next section.

4.3 Remaining challenges in coastal water

At global scale, the comparison between altimeter data and modeled H_{m0} results in a NRMSE of 11.6%. In coastal zones, the comparison against *in situ* data shows H_{m0} NRMSE values between 9% and 22%, i.e generally consistent with the error observed in surrounding deep waters. Very close to shore and in shallow depths (La Reunion and New-Caledonia), the model

also shows comparable predictive skills which demonstrates that the wave transformations from deep to shallow water are correctly simulated, despite challenges associated with the presence of steep-slope. Both modeled wave periods T_{m02} and T_p display similar accuracy than for H_{m0} (NRMSE values<20%) although T_p remains more unstable under multi-modal sea states.

In coastal zones, the underestimation of the energy spectrum below 0.04 Hz that can be seen on Fig.14 and 12 can be attributed to the presence of infragravity waves (see Bertin et al. (2018) for a recent review), which are not represented in the present model. At Grande Vigie station (Fig. 12), the 90 m water depth implies that energy in the IG wave band corresponds to free IG waves reflected along the coast, a problem discussed by Alday et al. (2021). Part of the discrepancies closest to shore can be attributed to the finest mesh resolution of 100 m (Fig. 13). Even though it is a very high refinement for a global model, it remains too crude to represent the rapidly varying bathymetry related to the complex reef (Buckley et al., 2016). In order to make clear recommendations concerning the minimum resolution required for such comparisons, we need more adequate measurements and we are waiting for forthcoming high-resolution simulations to carry out comparative studies. Additionally, the issue of resolution remains closely tied to interpolation issues when comparing measurements and model in rapidly varying media.

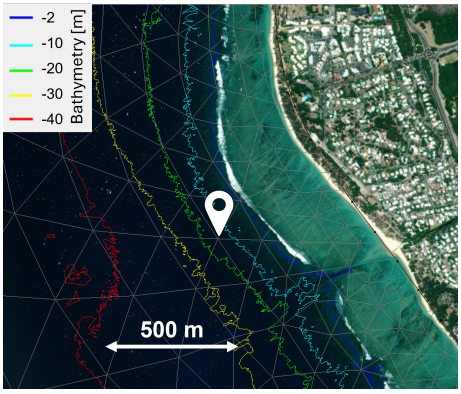

Figure 13. Satellite view of the Hermitage fringing reef (La Reunion Island) with the extension of the model grid, a detailed bathymetry map (extracted from "Litto3D" LiDAR data (IGN/SHOM)) and the location of the pressure sensor on the reef.

The steep bathymetries usually bordering tropical islands (with bottom slope locally easily exceeding 1:10) pose an additional challenge for spectral models. Indeed, spectral models are based on the wave action equation, which was derived for waves propagating in "slowly varying media" (Bretherton et al., 1968), a condition that is not met for such steep slopes.

When the waves approach the coast, triad interactions transfer energy from the peak frequency to lower (subharmonics) and higher (superharmonic) frequencies. In this model, the Lumped Triad Approximation (LTA) of Eldeberky (1996) is used to reproduce the energy transfer towards higher frequencies. Although widely used, the LTA is a crude approximation and can only represent the second harmonic, which can result in high energy differences at high frequencies as seen in Fig. 14. The

mean period T_{m02} being sensitive to high frequencies, this problem could explain why we have higher errors on this parameter in shallow depths (as seen in Fig. 7).

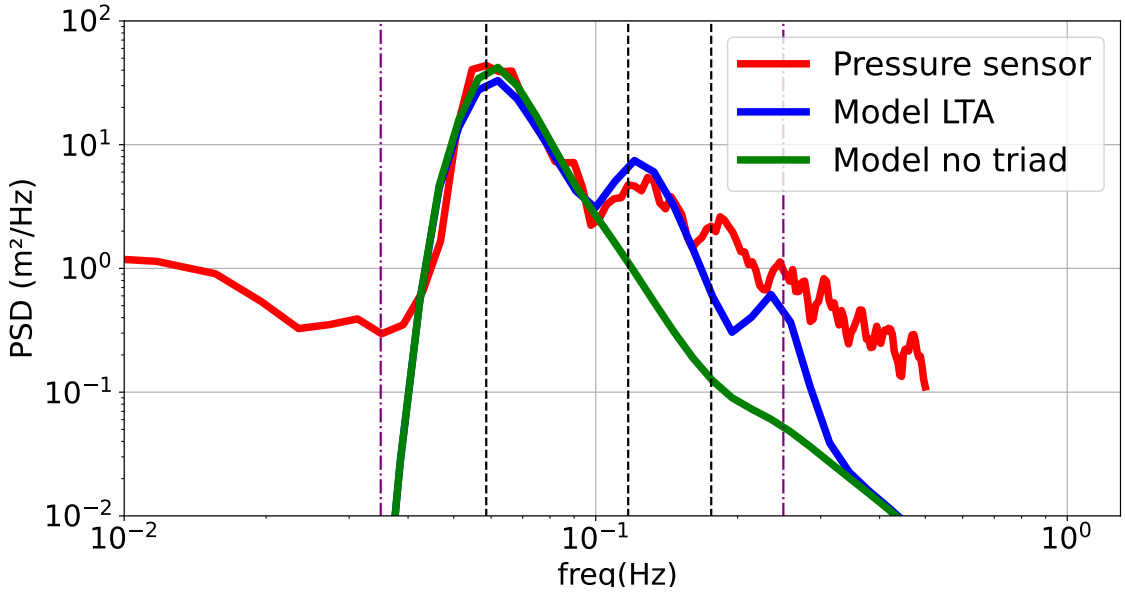

Figure 14. Comparison between power spectral density derived from pressure measurements (red) and modeled with (blue) and without (green) triads at 9:00 UTC on June 8th, 2022 (Hermitage, La Reunion Island). The purple lines represent the cut-off frequencies. The black lines represent the peak frequency and the superharmonic frequencies.

5 Conclusions

A new global high resolution wave model for the tropical ocean is presented in this paper. The model aims at better simulating the sea state in the tropical ocean, which requires to capture the large extent of DSS propagation (i.e global model) while having a high local refinement to represent explicitly islands (i.e high refinement). Our approach combines the use of unstructured grid, with a global resolution of 50 km refined down to 100 m in nearshore areas of interest, and an implicit scheme which substantially reduces computational cost. In addition, we develop a new quantile-quantile correction for the ERA5 wind, resulting in small biases for most wave heights. In addition to classic validation in deep waters against satellite altimetry data, this modeling strategy allows for the first time to perform direct comparisons in shallow depth, that is very close to shore due to the steep slopes usually surrounding tropical islands.

Despite difficulties related to the possible diffusion of the implicit scheme and the representation of nonlinear interactions, the model gives promising results with a correct representation of the wave transformation, from deep to shallow water. The availability of long-term *in situ* data remains one of the main challenges to validate wave models in tropical volcanic islands. The lack of wave measurements is usually due to the combination of remote location, difficult access, very steep seabed slopes

and strong exposure to waves, which makes deployment in shallow areas even more challenging. The availability of spectrum data is particularly helpful in understanding the origins of possible discrepancies between model and observations. In addition to the need to pursue the deployment of local *in situ* surveys, the new satellite data, such as the recently launched Surface Water and Ocean Topography (SWOT) mission, should provide useful high resolution wave measurements close to shore (Chelton et al., 2022) and facilitate validation of global and coastal models.

Code and data availability. Model setup files for the unstructured grid can be accessed at https://doi.org/10.5281/zenodo.13341123. The version 7.14 of WAVEWATCHIII is available here https://github.com/NOAA-EMC/WW3. Specifically, the code used in this work can be found at 10.5281/zenodo.14011562.

Author contributions. A. Gaffet: Conceptualization, Methodology, Software, Writing - original draft. X. Bertin: Conceptualization, Methodology, Software, Writing - review & editing, Supervision. D. Sous: Conceptualization, Writing - review & editing, Supervision. H. Michaud: Software, Writing - review & editing. E. Cordier: Data curation, Writing - review & editing . A. Roland: Software, Writing - review & editing.

Competing interests. The authors declare that they have no conflict of interest.

Acknowledgements. A. Gaffet is supported by a PhD fellowship from the CREOCEAN engineering consulting company. This research is also funded by the France 2030 PPR Ocean and Climate project FUTURISKS (ANR-22-POCE-0002). Permanent pressure data are collected on the reef slope at the Hermitage in the scope of the National Observation Service DYNALIT, part of the Research Infrastructure ILICO. We are very grateful to the CEREMA and the NDBC for sharing wave buoy data. We also thank the GEOCEAN-NC campaign for their pressure sensor data. The authors acknowledge the WW3 IFREMER/LOPS team for making available their satellite/model comparison Fortran routine and Dr Swen Jullien for usefull advices regarding radiometer wind data. We are also thankful for the support of the Fondation de la Mer. This project was provided with computing HPC and storage resources by GENCI at IDRIS thanks to the grant 2023-AD010114543 on the supercomputer Jean Zay CSL partition.

References

Abdolali, A., Roland, A., Van Der Westhuysen, A., Meixner, J., Chawla, A., Hesser, T. J., Smith, J. M., and Sikiric, M. D.: Large-scale hurricane modeling using domain decomposition parallelization and implicit scheme implemented in WAVEWATCH III wave model, Coastal Engineering, 157, 103 656, https://doi.org/10.1016/j.coastaleng.2020.103656, 2020.

Abdolali, A., van der Westhuysen, A., Ma, Z., Mehra, A., Roland, A., and Moghimi, S.: Evaluating the accuracy and uncertainty of atmospheric and wave model hindcasts during severe events using model ensembles, Ocean Dynamics, 71, 217–235, https://doi.org/10.1007/s10236-020-01426-9, 2021.

Abdolali, A., Hesser, T. J., Anderson Bryant, M., Roland, A., Khalid, A., Smith, J., Ferreira, C., Mehra, A., and Sikiric, M. D.: Wave Attenuation by Vegetation: Model Implementation and Validation Study, Frontiers in Built Environment, 8, 891 612, https://doi.org/10.3389/fbuil.2022.891612, 2022.

Alday, M. and Ardhuin, F.: On Consistent Parameterizations for Both Dominant Wind-Waves and Spectral Tail Directionality, Journal of Geophysical Research: Oceans, 128, e2022JC019 581, https://doi.org/10.1029/2022JC019581, _eprint: https://onlinelibrary.wiley.com/doi/pdf/10.1029/2022JC019581, 2023.

Alday, M., Accensi, M., Ardhuin, F., and Dodet, G.: A global wave parameter database for geophysical applications. Part 3: Improved forcing and spectral resolution, Ocean Modelling, 166, 101 848, https://doi.org/10.1016/j.ocemod.2021.101848, 2021.

Alves, J.-H., Tolman, H., Roland, A., Abdolali, A., Ardhuin, F., Mann, G., Chawla, A., and Smith, J.: NOAA's Great Lakes Wave Prediction System: A Successful Framework for Accelerating the Transition of Innovations to Operations, Bulletin of the American Meteorological Society, 104, https://doi.org/10.1175/BAMS-D-22-0094.1, 2022.

Andréfouët, S., Bruyère, O., Liao, V., and Le Gendre, R.: Hydrodynamical impact of the July 2022 'Code Red' distant mega-swell on Apataki Atoll, Tuamotu Archipelago, Global and Planetary Change, 228, 104 194, https://doi.org/10.1016/j.gloplacha.2023.104194, 2023.

Ardhuin, F., O'Reilly, W. C., Herbers, T. H. C., and Jessen, P. F.: Swell Transformation across the Continental Shelf. Part I: Attenuation and Directional Broadening, Journal of Physical Oceanography, 33, 1921–1939, https://doi.org/10.1175/1520-0485(2003)033<1921:STATCS>2.0.CO;2, publisher: American Meteorological Society Section: Journal of Physical Oceanography, 2003.

Ardhuin, F., Rogers, E., Babanin, A., Filipot, J.-F., Magne, R., Roland, A., Van Der Westhuysen, A., Queffeulou, P., Lefevre, J.-M., Aouf, L., and Collard, F.: Semi-empirical dissipation source functions for ocean waves: Part I, definition, calibration and validation, Journal of Physical Oceanography, 40, 1917–1941, https://doi.org/10.1175/2010JPO4324.1, arXiv:0907.4240 [physics], 2010.

Ardhuin, F., Tournadre, J., Queffeulou, P., Girard-Ardhuin, F., and Collard, F.: Observation and parameterization of small icebergs: Drifting breakwaters in the southern ocean, Ocean Modelling, 39, 405–410, https://doi.org/10.1016/j.ocemod.2011.03.004, 2011.

Ardhuin, F., Collard, F., Chapron, B., Girard-Ardhuin, F., Guitton, G., Mouche, A., and Stopa, J. E.: Estimates of ocean wave heights and attenuation in sea ice using the SAR wave mode on Sentinel-1A, Geophysical Research Letters, 42, 2317–2325, https://doi.org/10.1002/2014GL062940, _eprint: https://onlinelibrary.wiley.com/doi/pdf/10.1002/2014GL062940, 2015.

Ardhuin, F., Gille, S. T., Menemenlis, D., Rocha, C. B., Rascle, N., Chapron, B., Gula, J., and Molemaker, J.: Small-scale open ocean currents have large effects on wind wave heights, Journal of Geophysical Research: Oceans, 122, 4500–4517, https://doi.org/10.1002/2016JC012413, 2017.

Battjes, J. A. and Janssen, J. P. F. M.: Energy Loss and Set-Up Due to Breaking of Random Waves, pp. 569–587, https://doi.org/10.1061/9780872621909.034, publisher: American Society of Civil Engineers, 1978.

Benoit, M.: IMPLEMENTATION AND TEST OF IMPROVED METHODS FOR EVALUATION OF NONLINEAR QUADRUPLET INTERACTIONS IN A THIRD GENERATION WAVE MODEL, in: Coastal Engineering 2006, pp. 526–538, World Scientific Publishing Company, San Diego, California, USA, ISBN 978-981-270-636-2 978-981-270-955-4, https://doi.org/10.1142/9789812709554_0046, 2007.

Bentamy, A. and Croize-Fillon, D.: Gridded surface wind fields from Metop/ASCAT measurements, International Journal Of Remote Sensing, 33, 1729–1754, https://doi.org/10.1080/01431161.2011.600348, publisher: Taylor & Francis Ltd, 2012.

Bertin, X., de Bakker, A., van Dongeren, A., Coco, G., André, G., Ardhuin, F., Bonneton, P., Bouchette, F., Castelle, B., Crawford, W. C., Davidson, M., Deen, M., Dodet, G., Guérin, T., Inch, K., Leckler, F., McCall, R., Muller, H., Olabarrieta, M., Roelvink, D., Ruessink, G., Sous, D., Stutzmann, , and Tissier, M.: Infragravity waves: From driving mechanisms to impacts, Earth-Science Reviews, 177, 774–799, https://doi.org/10.1016/j.earscirev.2018.01.002, 2018.

Biscara, L. and Maspataud, A.: France d'outre-mer : mise à disposition d'une nouvelle gamme de MNT bathymétriques de référence, https://doi.org/10.13140/RG.2.2.29381.47840, publisher: [object Object], 2018.

Booij, N., Ris, R. C., and Holthuijsen, L. H.: A third-generation wave model for coastal regions: 1. Model description and validation, Journal of Geophysical Research: Oceans, 104, 7649–7666, https://doi.org/10.1029/98JC02622, _eprint: https://onlinelibrary.wiley.com/doi/pdf/10.1029/98JC02622, 1999.

Bretherton, F. P., Garrett, C. J. R., and Lighthill, M. J.: Wavetrains in inhomogeneous moving media, Proceedings of the Royal Society of London. Series A. Mathematical and Physical Sciences, 302, 529–554, https://doi.org/10.1098/rspa.1968.0034, publisher: Royal Society, 1968.

Brus, S. R., Wolfram, P. J., Van Roekel, L. P., and Meixner, J. D.: Unstructured global to coastal wave modeling for the Energy Exascale Earth System Model using WAVEWATCH III version 6.07, Geoscientific Model Development, 14, 2917–2938, https://doi.org/10.5194/gmd-14-2917-2021, number: 5 Publisher: Copernicus GmbH, 2021.

Buckley, M. L., Lowe, R. J., Hansen, J. E., and Van Dongeren, A. R.: Wave Setup over a Fringing Reef with Large Bottom Roughness, Journal of Physical Oceanography, 46, 2317–2333, https://doi.org/10.1175/JPO-D-15-0148.1, number: 8, 2016.

Campos, R. M., Gramcianinov, C. B., de Camargo, R., and da Silva Dias, P. L.: Assessment and Calibration of ERA5 Severe Winds in the Atlantic Ocean Using Satellite Data, Remote Sensing, 14, 4918, https://doi.org/10.3390/rs14194918, number: 19 Publisher: Multidisciplinary Digital Publishing Institute, 2022.

Canavesio, R.: Distant swells and their impacts on atolls and tropical coastlines. The example of submersions produced by lagoon water filling and flushing currents in French Polynesia during 1996 and 2011 mega swells, Global and Planetary Change, 177, 116–126, https://doi.org/10.1016/j.gloplacha.2019.03.018, 2019.

Chelton, D. B., Schlax, M. G., Freilich, M. H., and Milliff, R. F.: Satellite Measurements Reveal Persistent Small-Scale Features in Ocean Winds, Science, 303, 978–983, https://doi.org/10.1126/science.1091901, 2004.

Chelton, D. B., Samelson, R. M., and Farrar, J. T.: The Effects of Uncorrelated Measurement Noise on SWOT Estimates of Sea Surface Height, Velocity, and Vorticity, Journal of Atmospheric and Oceanic Technology, 39, 1053–1083, https://doi.org/10.1175/JTECH-D-21-0167.1, publisher: American Meteorological Society Section: Journal of Atmospheric and Oceanic Technology, 2022.

Chupin, C., Ballu, V., Testut, L., Tranchant, Y.-T., and Aucan, J.: Nouméa: a new multi-mission calibration and validation site for past and future altimetry missions?, Ocean Science, 19, 1277–1314, https://doi.org/10.5194/os-19-1277-2023, publisher: Copernicus GmbH, 2023.

Cooper, J., Jackson, D., and Gore, S.: A groundswell event on the coast of the British Virgin Islands: spatial variability in morphological impact, Journal of Coastal Research, 65, 696–701, https://doi.org/10.2112/SI65-118.1, 2013.

Cordier, E., Jaquemet, S., Benoit, Y., David, M., Ferreira, S., Stamenoff, P., Bigot, L., Bureau, S., Fiat, S., menkes, c., Varillon, D., and Hocdé, R.: ReefTEMPS-OI - The Indian Ocean Island coastal ocean observation network, https://doi.org/10.26171/7PCX-VM26, 2024.

Delpey, M. T., Ardhuin, F., Collard, F., and Chapron, B.: Space-time structure of long ocean swell fields, Journal of Geophysical Research: Oceans, 115, https://doi.org/10.1029/2009JC005885, number: C12 _eprint: https://onlinelibrary.wiley.com/doi/pdf/10.1029/2009JC005885, 2010.

Dodet, G., Piolle, J.-F., Quilfen, Y., Abdalla, S., Accensi, M., Ardhuin, F., Ash, E., Bidlot, J.-R., Gommenginger, C., Marechal, G., Passaro, M., Quartly, G., Stopa, J., Timmermans, B., Young, I., Cipollini, P., and Donlon, C.: The Sea State CCI dataset v1: towards a sea state climate data record based on satellite observations, Earth System Science Data, 12, 1929–1951, https://doi.org/10.5194/essd-12-1929-2020, publisher: Copernicus GmbH, 2020.

Dutheil, C., Andrefouët, S., Jullien, S., Le Gendre, R., Aucan, J., and Menkes, C.: Characterization of south central Pacific Ocean wind regimes in present and future climate for pearl farming application, Marine Pollution Bulletin, 160, 111 584, https://doi.org/10.1016/j.marpolbul.2020.111584, 2020.

Dörenkämper, M., Olsen, B. T., Witha, B., Hahmann, A. N., Davis, N. N., Barcons, J., Ezber, Y., García-Bustamante, E., González-Rouco, J. F., Navarro, J., Sastre-Marugán, M., Sīle, T., Trei, W., Žagar, M., Badger, J., Gottschall, J., Sanz Rodrigo, J., and Mann, J.: The Making of the New European Wind Atlas – Part 2: Production and evaluation, Geoscientific Model Development, 13, 5079–5102, https://doi.org/10.5194/gmd-13-5079-2020, 2020.

Eldeberky, Y.: Nonlinear transformation of Wave Spectra in the Nearshore Zone., 1996.

Ferziger, J. and Peric, M.: Computational Methods for Fluid Dynamics / J.H. Ferziger, M. Peric., vol. 3, ISBN 978-3-540-42074-3, https://doi.org/10.1007/978-3-642-56026-2, journal Abbreviation: Computational Methods for Fluid Dynamics Publication Title: Computational Methods for Fluid Dynamics, 2002.

Ford, M., Merrifield, M. A., and Becker, J. M.: Inundation of a low-lying urban atoll island: Majuro, Marshall Islands, Natural Hazards, 91, 1273–1297, https://doi.org/10.1007/s11069-018-3183-5, 2018.

Gattuso, J.-P., Brewer, P., Hoegh-Guldberg, O., Kleypas, J., Pörtner, H.-O., and Schmidt, D.: Cross-chapter box on Ocean acidification, pp. 129–131, 2014.

Giardino, A., Nederhoff, K., and Vousdoukas, M.: Coastal hazard risk assessment for small islands: assessing the impact of climate change and disaster reduction measures on Ebeye (Marshall Islands), Regional Environmental Change, 18, 2237–2248, https://doi.org/10.1007/s10113-018-1353-3, number: 8, 2018.

Graf, M., Scherrer, S. C., Schwierz, C., Begert, M., Martius, O., Raible, C. C., and Brönnimann, S.: Near-surface mean wind in Switzerland: Climatology, climate model evaluation and future scenarios, International Journal of Climatology, 39, 4798–4810, https://doi.org/10.1002/joc.6108, 2019.

Gutiérrez, C., Molina, M., Ortega, M., López-Franca, N., and Sánchez, E.: Low-wind climatology (1979–2018) over Europe from ERA5 reanalysis, Climate Dynamics, 62, 4155–4170, https://doi.org/10.1007/s00382-024-07123-3, 2024.

Hasselmann, S. and Hasselmann, K.: Computations and parameterizations of the nonlinear energy transfer in a gravity-wave spectrum. Part I: A new method for efficient computations of the exact nonlinear transfer integral, Journal of Physical Oceanography, 15, 1369–1377, https://doi.org/10.1175/1520-0485(1985)015<1369:CAPOTN>2.0.CO;2, publisher: American Meteorological Society, 1985.

Hasselmann, S., Hasselmann, K., Allender, J. H., and Barnett, T. P.: Computations and parameterizations of the nonlinear energy transfer in a gravity-wave spectrum. Part II: Parameterizations of the nonlinear energy transfer for application in wave models, Journal of Physical

Oceanography, 15, 1378–1391, https://doi.org/10.1175/1520-0485(1985)015<1378:CAPOTN>2.0.CO;2, publisher: American Meteorological Society, 1985.

Hersbach, H. and Janssen, P. a. E. M.: Improvement of the Short-Fetch Behavior in the Wave Ocean Model (WAM), Journal of Atmospheric and Oceanic Technology, 16, 884–892, https://doi.org/10.1175/1520-0426(1999)016<0884:IOTSFB>2.0.CO;2, publisher: American Meteorological Society Section: Journal of Atmospheric and Oceanic Technology, 1999.

Hersbach, H., Bell, B., Berrisford, P., Hirahara, S., Horányi, A., Muñoz-Sabater, J., Nicolas, J., Peubey, C., Radu, R., Schepers, D., Simmons, A., Soci, C., Abdalla, S., Abellan, X., Balsamo, G., Bechtold, P., Biavati, G., Bidlot, J., Bonavita, M., De Chiara, G., Dahlgren, P., Dee, D., Diamantakis, M., Dragani, R., Flemming, J., Forbes, R., Fuentes, M., Geer, A., Haimberger, L., Healy, S., Hogan, R. J., Hólm, E., Janisková, M., Keeley, S., Laloyaux, P., Lopez, P., Lupu, C., Radnoti, G., de Rosnay, P., Rozum, I., Vamborg, F., Villaume, S., and Thépaut, J.-N.: The ERA5 global reanalysis, Quarterly Journal of the Royal Meteorological Society, 146, 1999–2049, https://doi.org/10.1002/qj.3803, number: 730 _eprint: https://onlinelibrary.wiley.com/doi/pdf/10.1002/qj.3803, 2020.

Hoeke, R. K., McInnes, K. L., Kruger, J. C., McNaught, R. J., Hunter, J. R., and Smithers, S. G.: Widespread inundation of Pacific islands triggered by distant-source wind-waves, Global and Planetary Change, 108, 128–138, https://doi.org/10.1016/j.gloplacha.2013.06.006, 2013.

Jullien, S., Aucan, J., Kestenare, E., Lengaigne, M., and Menkes, C.: Unveiling the global influence of tropical cyclones on extreme waves approaching coastal areas, Nature Communications, 15, 6593, https://doi.org/10.1038/s41467-024-50929-2, 2024.

Karypis, G.: METIS and ParMETIS, in: Encyclopedia of Parallel Computing, edited by Padua, D., pp. 1117–1124, Springer US, Boston, MA, ISBN 978-0-387-09766-4, https://doi.org/10.1007/978-0-387-09766-4_500, 2011.

Kennedy, A. B., Westerink, J. J., Smith, J. M., Hope, M. E., Hartman, M., Taflanidis, A. A., Tanaka, S., Westerink, H., Cheung, K. F., Smith, T., Hamann, M., Minamide, M., Ota, A., and Dawson, C.: Tropical cyclone inundation potential on the Hawaiian Islands of Oahu and Kauai, Ocean Modelling, 52-53, 54–68, https://doi.org/10.1016/j.ocemod.2012.04.009, 2012.

Khan, S. S., Echevarria, E. R., and Hemer, M. A.: Ocean Swell Comparisons Between Sentinel-1 and WAVEWATCH III Around Australia, Journal of Geophysical Research: Oceans, 126, e2020JC016 265, https://doi.org/10.1029/2020JC016265, _eprint: https://onlinelibrary.wiley.com/doi/pdf/10.1029/2020JC016265, 2021.

Komen, G. J., Cavaleri, L., Donelan, M., Hasselmann, K., Hasselmann, S., and Janssen, P. A. E. M.: Dynamics and Modelling of Ocean Waves, https://ui.adsabs.harvard.edu/abs/1996dmow.book.....K, publication Title: Dynamics and Modelling of Ocean Waves ADS Bibcode: 1996dmow.book.....K, 1996.

Lecacheux, S., Pedreros, R., Le Cozannet, G., Thiébot, J., De La Torre, Y., and Bulteau, T.: A method to characterize the different extreme waves for islands exposed to various wave regimes: a case study devoted to Reunion Island, Natural Hazards and Earth System Sciences, 12, 2425–2437, https://doi.org/10.5194/nhess-12-2425-2012, 2012.

Lefèvre, J.-M.: High swell warnings in the Caribbean Islands during March 2008, Natural Hazards, 49, 361–370, https://doi.org/10.1007/s11069-008-9323-6, 2009.

Leonard, B. P.: The ULTIMATE conservative difference scheme applied to unsteady one-dimensional advection, Computer Methods in Applied Mechanics and Engineering, 88, 17–74, https://doi.org/10.1016/0045-7825(91)90232-U, 1991.

Liu, A. K. and Mollo-Christensen, E.: Wave Propagation in a Solid Ice Pack, Journal of Physical Oceanography, 18, 1702–1712, https://doi.org/10.1175/1520-0485(1988)018<1702:WPIASI>2.0.CO;2, publisher: American Meteorological Society Section: Journal of Physical Oceanography, 1988.

Liu, A. K., Holt, B., and Vachon, P. W.: Wave propagation in the marginal ice zone: Model predictions and comparisons with buoy and synthetic aperture radar data, Journal of Geophysical Research, 96, 4605–4621, https://doi.org/10.1029/90JC02267, aDS Bibcode: 1991JGR....96.4605L, 1991.

Liu, Q., Babanin, A. V., Rogers, W. E., Zieger, S., Young, I. R., Bidlot, J., Durrant, T., Ewans, K., Guan, C., Kirezci, C., Lemos, G., MacHutchon, K., Moon, I., Rapizo, H., Ribal, A., Semedo, A., and Wang, J.: Global Wave Hindcasts Using the Observation-Based Source Terms: Description and Validation, Journal of Advances in Modeling Earth Systems, 13, e2021MS002 493, https://doi.org/10.1029/2021MS002493, 2021.

Marechal, G. and Ardhuin, F.: Surface Currents and Significant Wave Height Gradients: Matching Numerical Models and High-Resolution Altimeter Wave Heights in the Agulhas Current Region, Journal of Geophysical Research: Oceans, 126, e2020JC016 564, https://doi.org/10.1029/2020JC016564, _eprint: https://onlinelibrary.wiley.com/doi/pdf/10.1029/2020JC016564, 2021.

Martins, K., Bonneton, P., Lannes, D., and Michallet, H.: Relation between Orbital Velocities, Pressure, and Surface Elevation in Nonlinear Nearshore Water Waves, Journal of Physical Oceanography, 51, 3539–3556, https://doi.org/10.1175/JPO-D-21-0061.1, publisher: American Meteorological Society Section: Journal of Physical Oceanography, 2021.

Masselink, G., Castelle, B., Scott, T., Dodet, G., Suanez, S., Jackson, D., and Floc'h, F.: Extreme wave activity during 2013/2014 winter and morphological impacts along the Atlantic coast of Europe, Geophysical Research Letters, 43, 2135–2143, https://doi.org/10.1002/2015GL067492, publisher: John Wiley & Sons, Ltd, 2016.

Masuda, A.: Nonlinear Energy Transfer Between Wind Waves, Journal of Physical Oceanography, 10, 2082–2093, https://doi.org/10.1175/1520-0485(1980)010<2082:NETBWW>2.0.CO;2, publisher: American Meteorological Society Section: Journal of Physical Oceanography, 1980.

Mentaschi, L., Kakoulaki, G., Vousdoukas, M., Voukouvalas, E., Feyen, L., and Besio, G.: Parameterizing unresolved obstacles with source terms in wave modeling: A real-world application, Ocean Modelling, 126, 77–84, https://doi.org/10.1016/j.ocemod.2018.04.003, 2018.

Mentaschi, L., Vousdoukas, M., Garcia-Sanchez, G., Montblanc, T. F., Voukouvalas, E., Federico, I., Abdolali, A., Zhang, Y. J., and Feyen, L.: A global unstructured, coupled, high- resolution hindcast of waves and storm surges, 2023.

Monteiro, N. M., Oliveira, T. C., Silva, P. A., and Abdolali, A.: Wind–wave characterization and modeling in the Azores Archipelago, Ocean Engineering, 263, 112 395, https://doi.org/10.1016/j.oceaneng.2022.112395, 2022.

Moon, I.-J., Ginis, I., Hara, T., and Thomas, B.: A Physics-Based Parameterization of Air–Sea Momentum Flux at High Wind Speeds and Its Impact on Hurricane Intensity Predictions, Mon. Wea. Rev., 135, 2869–2878, https://doi.org/10.1175/MWR3432.1, 2007.

Moukalled, F., Mangani, L., and Darwish, M.: Erratum to: The Finite Volume Method in Computational Fluid Dynamics, in: The Finite Volume Method in Computational Fluid Dynamics, vol. 113, pp. E1–E1, Springer International Publishing, Cham, ISBN 978-3-319-16873-9 978-3-319-16874-6, https://doi.org/10.1007/978-3-319-16874-6_21, series Title: Fluid Mechanics and Its Applications, 2016.

Munk, W. H., Miller, G. R., Snodgrass, F. E., Barber, N. F., and Deacon, G. E. R.: Directional recording of swell from distant storms, Philosophical Transactions of the Royal Society of London. Series A, Mathematical and Physical Sciences, 255, 505–584, https://doi.org/10.1098/rsta.1963.0011, publisher: Royal Society, 1997.

Oppenheimer, M., Glavovic, B. C., Hinkel, J., van de Wal, R., Magnan, A. K., Abd-Elgawad, A., Cai, R., Cifuentes-Jara, M., Rica, C., DeConto, R. M., Ghosh, T., Hay, J., Islands, C., Isla, F., Marzeion, B., Meyssignac, B., Sebesvari, Z., Biesbroek, R., Buchanan, M. K., de Campos, R. S., Cozannet, G. L., Domingues, C., Dangendorf, S., Döll, P., Duvat, V. K. E., Edwards, T., Ekaykin, A., Frederikse, T., Gattuso, J.-P., Kopp, R., Lambert, E., Lawrence, J., Narayan, S., Nicholls, R. J., Renaud, F., Simm, J., Smit, A., Woodruff, J., Wong, P. P.,

Xian, S., Abe-Ouchi, A., Gupta, K., and Pereira, J.: Sea Level Rise and Implications for Low-Lying Islands, Coasts and Communities, 2019.

Pineau-Guillou, L., Ardhuin, F., Bouin, M.-N., Redelsperger, J.-L., Chapron, B., Bidlot, J.-R., and Quilfen, Y.: Strong winds in a coupled wave–atmosphere model during a North Atlantic storm event: evaluation against observations, Quarterly Journal of the Royal Meteorological Society, 144, 317–332, https://doi.org/10.1002/qj.3205, _eprint: https://onlinelibrary.wiley.com/doi/pdf/10.1002/qj.3205, 2018.

Quilfen, Y. and Chapron, B.: On denoising satellite altimeter measurements for high-resolution geophysical signal analysis, Advances in Space Research, 68, 875–891, https://doi.org/10.1016/j.asr.2020.01.005, 2021.

Rapizo, H., Durrant, T. H., and Babanin, A. V.: An assessment of the impact of surface currents on wave modeling in the Southern Ocean, Ocean Dynamics, 68, 939–955, https://doi.org/10.1007/s10236-018-1171-7, 2018.

Rascle, N. and Ardhuin, F.: A global wave parameter database for geophysical applications. Part 2: Model validation with improved source term parameterization, Ocean Modelling, 70, 174–188, https://doi.org/10.1016/j.ocemod.2012.12.001, 2013.

Renfrew, I. A., Barrell, C., Elvidge, A. D., Brooke, J. K., Duscha, C., King, J. C., Kristiansen, J., Cope, T. L., Moore, G. W. K., Pickart, R. S., Reuder, J., Sandu, I., Sergeev, D., Terpstra, A., Våge, K., and Weiss, A.: An evaluation of surface meteorology and fluxes over the Iceland and Greenland Seas in ERA5 reanalysis: The impact of sea ice distribution, Quarterly Journal of the Royal Meteorological Society, 147, 691–712, https://doi.org/10.1002/qj.3941, _eprint: https://onlinelibrary.wiley.com/doi/pdf/10.1002/qj.3941, 2021.

Roland, A.: Development of WWM II: Spectral wave modeling on unstructured meshes, Ph.D. thesis, 2008.

Roland, A. and Ardhuin, F.: On the developments of spectral wave models: numerics and parameterizations for the coastal ocean, Ocean Dynamics, 64, 833–846, https://doi.org/10.1007/s10236-014-0711-z, 2014.

Samou, M. S., Bertin, X., Sakho, I., Lazar, A., Sadio, M., and Diouf, M. B.: Wave Climate Variability along the Coastlines of Senegal over the Last Four Decades, Atmosphere, 14, 1142, https://doi.org/10.3390/atmos14071142, 2023.

Schlembach, F., Passaro, M., Quartly, G. D., Kurekin, A., Nencioli, F., Dodet, G., Piollé, J.-F., Ardhuin, F., Bidlot, J., Schwatke, C., Seitz, F., Cipollini, P., and Donlon, C.: Correction: Schlembach, F., et al. Round Robin Assessment of Radar Altimeter Low Resolution Mode and Delay-Doppler Retracking Algorithms for Significant Wave Height. Remote Sens. 2020, 12, 1254, Remote Sensing, 13, 1182, https://doi.org/10.3390/rs13061182, number: 6 Publisher: Multidisciplinary Digital Publishing Institute, 2021.

Smithers, S. and Hoeke, R.: Geomorphological impacts of high-latitude storm waves on low-latitude reef islands — Observations of the December 2008 event on Nukutoa, Takuu, Papua New Guinea, Geomorphology, 222, 106–121, https://doi.org/10.1016/j.geomorph.2014.03.042, 2014.

Stopa, J. E. and Cheung, K. F.: Intercomparison of wind and wave data from the ECMWF Reanalysis Interim and the NCEP Climate Forecast System Reanalysis, Ocean Modelling, 75, 65–83, https://doi.org/10.1016/j.ocemod.2013.12.006, 2014.

Stopa, J. E., Ardhuin, F., and Girard-Ardhuin, F.: Wave climate in the Arctic 1992–2014: seasonality and trends, The Cryosphere, 10, 1605–1629, https://doi.org/10.5194/tc-10-1605-2016, publisher: Copernicus GmbH, 2016.

Tolman, H. L.: Treatment of unresolved islands and ice in wind wave models q, Ocean Modelling, 2003.

Tracy, B. and Resio, D.: Theory and Calculation of the Nonlinear Energy Transfer between Sea Waves in Deep Water., Tech. rep., https://apps.dtic.mil/sti/citations/ADA117989, section: Technical Reports, 1982.

Vledder, G. P. v., Herbers, T. H. C., Jensen, R. J., Resio, D. T., and Tracy, B.: Modelling of Non-Linear Quadruplet Wave-Wave Interactions in Operational Wave Models, pp. 797–811, https://doi.org/10.1061/40549(276)62, publisher: American Society of Civil Engineers, 2012.

Weatherall, P., Marks, K. M., Jakobsson, M., Schmitt, T., Tani, S., Arndt, J. E., Rovere, M., Chayes, D., Ferrini, V., and Wigley, R.: A new digital bathymetric model of the world's oceans, Earth and Space Science, 2, 331–345, https://doi.org/10.1002/2015EA000107, _eprint: https://onlinelibrary.wiley.com/doi/pdf/10.1002/2015EA000107, 2015.

Webb, D. J.: Non-linear transfers between sea waves, Deep Sea Research, 25, 279–298, https://doi.org/10.1016/0146-6291(78)90593-3, 1978.

Xie, S. P., Liu, W. T., Liu, Q., and Nonaka, M.: Far-reaching effects of the Hawaiian Islands on the Pacific Ocean-atmosphere system, Science (New York, N.Y.), 292, 2057–2060, https://doi.org/10.1126/science.1059781, 2001.

Zheng, K., Sun, J., Guan, C., and Shao, W.: Analysis of the Global Swell and Wind Sea Energy Distribution Using WAVEWATCH III, Advances in Meteorology, 2016, 8419 580, https://doi.org/10.1155/2016/8419580, _eprint: https://onlinelibrary.wiley.com/doi/pdf/10.1155/2016/8419580, 2016.